

Toward achieving cost-effective hexagonal BN semi-bulk crystals and BN neutron detectors via halide vapor phase epitaxy

Cite as: Appl. Phys. Lett. **122**, 012105 (2023); doi: 10.1063/5.0134858

Submitted: 14 November 2022 · Accepted: 20 December 2022 ·

Published Online: 5 January 2023



View Online



Export Citation



CrossMark

Z. Alemoush,  N. K. Hossain,  A. Tingsuwatit, M. Almohammad,  J. Li,  J. Y. Lin,^{a)}  and H. X. Jiang^{a)} 

AFFILIATIONS

Department of Electrical and Computer Engineering, Texas Tech University, Lubbock, Texas 79409, USA

^{a)} Authors to whom correspondence should be addressed: hx.jiang@ttu.edu and jingyu.lin@ttu.edu

ABSTRACT

Presently, thermal neutron detectors fabricated from boron-10 enriched hexagonal boron nitride (h-¹⁰BN) ultrawide bandgap semiconductor grown by metal organic chemical vapor deposition (MOCVD) hold the record high detection efficiency among all solid-state detectors at 59%. To overcome the short comings of MOCVD growth, including inherently low growth rate and unavoidable impurities such as carbon in metal organic source, we demonstrate here the growth of natural hexagonal boron nitride (h-BN) semi-bulk wafers using halide vapor phase epitaxy (HVPE), which is an established technique for producing GaN semi-bulk crystals at a high growth rate. Electrical transport characterization results revealed that these HVPE grown materials possess an electrical resistivity of $1 \times 10^{13} \Omega \text{ cm}$, and a charge carrier mobility and lifetime product of $2 \times 10^{-4} \text{ cm}^2/\text{V s}$. Detectors fabricated from a 100 μm thick h-BN wafer have demonstrated a thermal neutron detection efficiency of 20%, corresponding to a charge collection efficiency of $\sim 60\%$ at an operating voltage of 500 V. This initial demonstration opens the door for mass producing high efficiency h-BN semiconductor neutron detectors at a reduced cost, which could create unprecedented applications in nuclear energy, national security, nuclear waste monitoring and management, the health care industry, and material sciences.

Published under an exclusive license by AIP Publishing. <https://doi.org/10.1063/5.0134858>

The development of III-nitride wide bandgap semiconductor technology has made a huge impact on society, ranging from the creation of white light to consumer electronics in an entirely new manner.¹ Among III-nitrides, hexagonal BN (h-BN) with an ultrawide bandgap ($\sim 6.0 \text{ eV}$) in the three-dimensional form is the least studied in terms of material growth and device applications,^{2–5} although few-layer h-BN has been widely utilized as a complementary dielectric substrate and gate for 2D electronics^{6–9} as well as a host for optically stable single photon emitters.^{10–13} One of the distinct properties that sets BN apart from conventional III-nitrides is that the isotope B-10 (¹⁰B) is one of only a few elements, which possess large interaction cross sections with thermal neutron (σ), where $\sigma = 3480 \text{ Barns}$ or $3.48 \times 10^{-21} \text{ cm}^2$ for B-10.^{14,15} The density of ¹⁰B atoms in 100% B-10 enriched h-BN (h-¹⁰BN) is $N(^{10}\text{B}) = 5.5 \times 10^{22}/\text{cm}^3$, which provides a thermal neutron absorption coefficient (α) and absorption length λ of α (h-¹⁰BN) = $N\sigma = 5.5 \times 10^{22} \times 3.48 \times 10^{-21} = 211.2 \text{ cm}^{-1}$ and λ (h-¹⁰BN) = $\alpha^{-1} = 47.3 \mu\text{m}$.^{16–21} Since boron has two natural stable isotopes, with an average of 20% and 80% of ¹⁰B and ¹¹B in natural abundance, respectively, the density of ¹⁰B atoms in natural h-BN is five times smaller than that in h-¹⁰BN, and, therefore, we have λ (h-BN) = $237 \mu\text{m}$.

It has been widely recognized recently by the wide bandgap semiconductor research community that h-BN is an ideal material for the realization of solid-state direct conversion thermal neutron detectors.²² The key material parameters of h-¹⁰BN produced by metal organic chemical vapor deposition (MOCVD), including the mobility-lifetime product, layer thickness, and electrical resistivity, all have been increased by several orders of magnitude over a period of several years.^{17–21} These improvements have enabled the realization of high-performance h-¹⁰BN semiconductor thermal neutron detectors.^{18–21} Presently, h-¹⁰BN thermal neutron detectors hold the record high detection efficiency among all solid-state detectors at 59% (for a 1 cm^2 detection area).²¹

Indirect-conversion semiconductor detectors via either coating a thin ⁶Li or ¹⁰B neutron conversion layer on a bulk semiconductor^{23–25} or the formation of micro-pillars in a bulk semiconductor filled with a ¹⁰B or ⁶Li neutron conversion material^{26–29} have been developed, with the former being commercialized. Compared to the indirect-conversion semiconductor detectors with a limited theoretical detection efficiency, neutron absorption and charge collection occur in the same h-BN layer. The theoretical detection efficiency of h-BN thermal neutron detectors scales with the h-BN layer thickness following

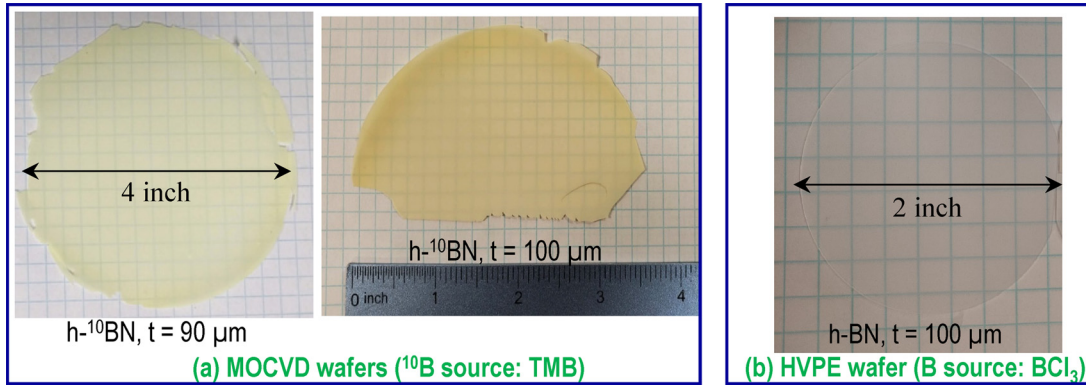


FIG. 1. Comparison of optical images of freestanding h-BN semi-bulk wafers: (a) 100% B-10 enriched h-BN ($h\text{-}^{10}\text{BN}$) wafers grown by MOCVD using trimethylboron (TMB) source as a precursor, all produced in authors' lab. Reproduced with permission from Maity *et al.*, Appl. Phys. Lett. **114**, 222102 (2019). Copyright 2019 AIP Publishing. Reproduced with permission from Maity *et al.*, Appl. Phys. Lett. **116**, 142102 (2020). Copyright 2020 AIP Publishing. (b) A h-BN wafer of 2-in. in diameter grown by HVPE using natural boron trichloride (BCl_3) gas as a precursor in the present work.

$$\eta_i(t) = 1 - e^{-t/\lambda}, \quad (1)$$

where t is the detector's layer thickness and λ is the thermal neutron absorption length, and therefore, η_i can approach 100% if the detector thickness is sufficiently large. So far, all high-performance neutron detectors were fabricated from $h\text{-}^{10}\text{BN}$ materials grown by MOCVD in authors' lab.^{18–21} While MOCVD growth technique is well-established for producing high quality III-nitride materials, its growth rate is limited (up to several micrometers per hour) and is best suited for fabricating photonic and electronic device structures.¹ The large thermal neutron absorption length, $\lambda(h\text{-}^{10}\text{BN}) = \alpha^{-1} = 47.3 \mu\text{m}$ or $\lambda(h\text{-BN}) = 237 \mu\text{m}$, makes the thickness requirement for the construction of high efficiency neutron detectors a great challenge for MOCVD epitaxial growth. The required long growth time translates to high cost. Additionally, the metal organic precursors used in MOCVD growth inevitably contain carbon impurities and sometimes even oxygen impurities, which are known to be deep level defects in h-BN³⁰ and are undesired for the performance of h-BN neutron detectors.^{16,18–21}

Halide vapor phase epitaxy (HVPE) growth is an established technique for producing semi-bulk GaN crystals in large wafer size at a high growth rate. More recently, HVPE growth technique has been employed to produce GaN vertical p–n junction devices with a significantly improved p-type conductivity control through the elimination of the residue carbon impurities.^{31,32} In this work, we report HVPE growth of natural h-BN. The detector fabricated from a $100 \mu\text{m}$ thick h-BN wafer delivered an overall detection efficiency of $\eta = 20\%$, corresponding to a charge collection efficiency of $\sim 60\%$. This initial demonstration opens the feasibility for producing cost-effective h-BN semi-bulk crystals and high efficiency h-BN semiconductor neutron detectors via HVPE.

To grow h-BN wafers, natural boron trichloride (BCl_3) and NH_3 were used as precursors. The growth was conducted on c-plane sapphire of 2-in. in diameter at a growth rate of about $25 \mu\text{m}/\text{h}$. Due to its layered structure, after growth during colling down, h-BN self-separates from sapphire to form a freestanding wafer.^{18–21} Figure 1 compares optical images among representative wafers (a) grown by MOCVD using B-10 enriched trimethylboron (TMB) metal organic

(MO) source as a precursor^{20,21} and (b) grown by HVPE in the present work. As can be seen from this side-by-side comparison, h-BN wafer grown by HVPE using BCl_3 gas as a precursor exhibits a much better transparency and less yellowish color than those produced by MOCVD using TMB source. The improved transparency is related to the fact that the BCl_3 precursor contains no carbon impurities. A previous theoretical work indicates that carbon impurities in h-BN can occupy both B and N sites as well on an interstitial site.³⁰ When occupying B site, C_B is a deep donor with an energy level of 2.2 eV below the conduction band edge, and when occupying an interstitial site, C_i is a deep acceptor sitting at an energy level of 2.4 eV above the valence band edge;³⁰ the presence of both of which will render a yellowish colored wafer. When occupied on N site, C_N is an extremely deep level acceptor with a transition energy of 3.2 eV to the valence band.³⁰ Figure 2 shows the x-ray diffraction (XRD) θ – 2θ scan, revealing a dominant diffraction peak at 26.7° , corresponding to a c-lattice

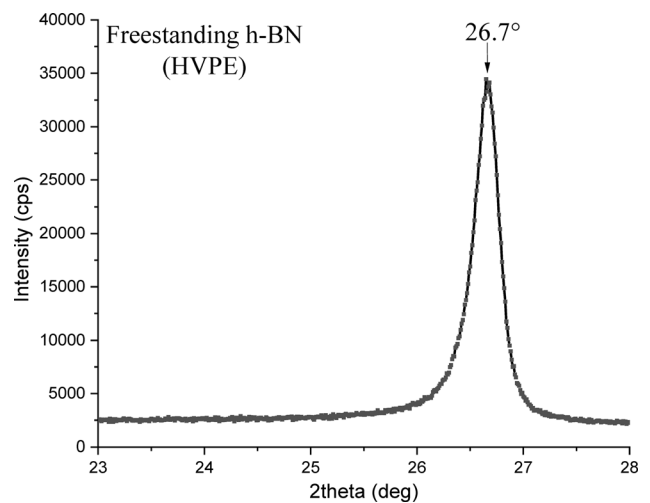


FIG. 2. XRD θ – 2θ scan of a freestanding h-BN semi-bulk wafer grown by HVPE using BCl_3 gas as a precursor.

constant of 6.67 Å, associated with the hexagonal phase of BN. The XRD spectral line shape is quite comparable to those of MOCVD grown h-¹⁰BN semi-bulk wafers reported earlier by our group.³³ In terms of optical properties, the room temperature photoluminescence emission spectra of HVPE semi-bulk wafers exhibit peaks associated with both the band edge and impurity transitions, while MOCVD grown semi-bulk crystals (> 30 μm) exhibit only transitions related to the deep level defects (see, e.g., Fig. 20, Ref. 16).

For the electrical property and neutron detection performance studies, lateral detectors were fabricated to take the advantages of h-BN's superior lateral transport properties over its vertical transport properties.¹⁶ The fabrication processes include the following steps: (1) dicing h-BN wafer into detector strips; (2) mount detector strips on sapphire using a highly resistive adhesive material; and (3) a mask was used to deposit metal contacts consisting of a bi-layer of Ni (100 nm)/Au (40 nm) on the clipped edges of the h-BN strips using e-beam evaporation, leaving around ~100 μm of metal covering on the two edges.^{20,21} The schematic illustration of these lateral detectors is depicted in Fig. 3(a). Figure 3(b) shows a micrograph of a fabricated detector strip (2 mm in width) mounted on sapphire via a layer of highly resistive and adhesive polyimide. Dark I-V characterization yields an electrical resistivity of 1.1×10^{13} Ω cm, which is comparable to those of MOCVD grown h-¹⁰BN.^{18–21}

One of the most important parameters for determining the charge collection efficiency of a neutron detector is its carrier mobility and lifetime product ($\mu\tau$).^{16–21} Most of the neutron-generated charge carriers inside a detector can be collected when the carrier recombination time (τ) is greater than the transit time (τ_t), $\tau > \tau_t$, or equivalently, the charge carrier drift length ($= \mu\tau E$) is greater than the carrier transit distance (or the width of the detector strip, W). This means that $\mu\tau E > W$ is the condition to ensure a high charge collection efficiency, where W is the width of the detector strip and E (V) is the applied electric field (bias voltage). The quantity of $\mu\tau$ is strongly influenced by the overall material quality. For MOCVD grown h-¹⁰BN, the $\mu\tau$ values measured under UV excitation have been improved by several orders of magnitude from 10^{-8} cm²/V (Ref. 17) to 5×10^{-3} cm²/V,²¹ leading to the realization of high-performance

neutron detectors.²¹ Since the growth of HVPE of h-BN is at an initial stage, it is desirable to benchmarking the $\mu\tau$ parameter against those of MOCVD grown materials. The photocurrent–voltage (I–V) characteristics under UV excitation were utilized to extract $\mu\tau$ value using the classical Many's equation for insulating semiconductors.³⁴ Since the contact area is small in a lateral detector, we neglected the effect of surface recombination and take into consideration only the bulk trapping effect, which yields an expression for the I–V characteristics under illumination as

$$I(V) = I_0 \left[\frac{\mu_n \tau_n V}{W^2} - \left(\frac{\mu_n \tau_n V}{W^2} \right)^2 \left(1 - e^{-\frac{W}{\mu_n \tau_n V}} \right) + \frac{\mu_p \tau_p V}{W^2} - \left(\frac{\mu_p \tau_p V}{W^2} \right)^2 \left(1 - e^{-\frac{W}{\mu_p \tau_p V}} \right) \right]. \quad (2)$$

The measured I–V characteristics under the illumination by a broad-spectrum UV (185 to 400 nm) light source are shown in Fig. 3(c). In fitting the data with Eq. (2), we assumed that the $\mu\tau$ product for electrons and holes is comparable ($\mu_n \tau_n = \mu_p \tau_p$) in the lateral direction¹⁶ for initial assessment. The fitting results provided a $\mu\tau$ value of 2×10^{-4} cm²/V, which is on the same order as the values of most MOCVD grown semi-bulk wafers^{16,18–20} and is sufficiently large to satisfy the charge collection condition of $\mu\tau E > W$ if we operate the detector at the same bias voltage of 500 V as in the previous best performing h-¹⁰BN detector.²¹ In the future, it would be interesting to measure the $\mu\tau$ products under an alpha source irradiation, which resembles more closely to the scenario of thermal neutron irradiation.

With the considerations discussed above, we carried out thermal neutron detection efficiency measurements. To do so, as described previously,^{16–21} a Californium-252 (²⁵²Cf) source from Frontier Technology was used as a neutron source. The calibrated fast neutron emission rate of ²⁵²Cf at the time of measurement was about 7.3×10^5 neutrons per second (n/s). A high-density polyethylene (HDPE) cube moderator with the front surface of 2.5 cm in thickness was used to house the neutron source and to convert fast neutrons to thermal neutrons. The h-BN detector and a commercial ⁶LiF filled 4 cm² micro-structured semiconductor neutron detector (MSND Domino™ V4)

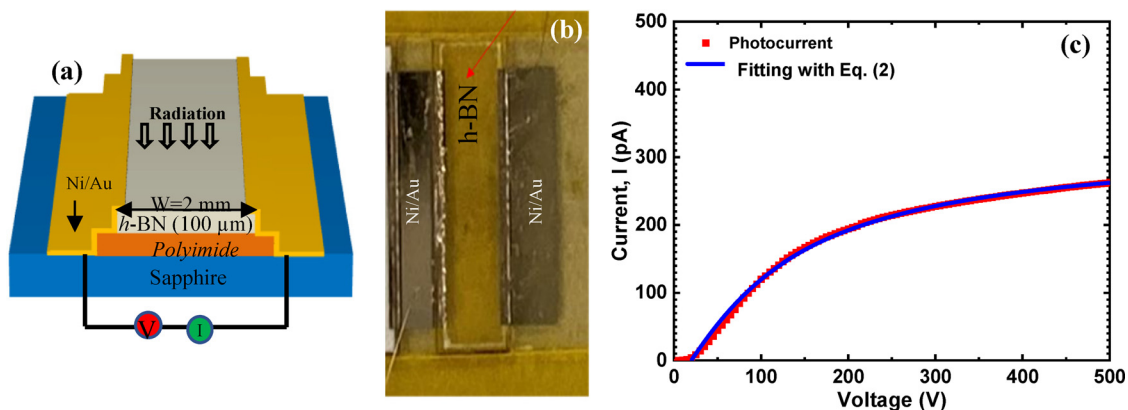


FIG. 3. (a) Schematic of a thermal neutron detector in lateral geometry fabricated from HVPE grown h-BN with a detector strip width of $W = 2$ mm. (b) Optical image of a fabricated thermal neutron detector in lateral geometry ($W = 2$ mm) fabricated from a 100 μm thick freestanding h-BN wafer grown by HVPE using natural boron trichloride (BCl_3) gas as a precursor. (c) I–V characteristics of the detector shown in (b) under the illumination by a broad-spectrum UV (185 to 400 nm) light source.

with a certified detection efficiency of 30% were placed side-by-side at 30 cm from the HDPE surface and exposed to thermal neutrons for the same duration of time, and the detection efficiency (η) of the h-BN detector can be obtained by calibrating the counts against that of MSND. Figure 4 shows the pulsed height spectra of a h-BN detector measured at 500 V. The spectrum (red) was measured under thermal neutron irradiation, and the dark spectrum (blue) was also recorded in the absence of any radiation. Calibration against the MSND detector provided a thermal neutron detection efficiency of $\eta = 20\%$ at 500 V for the detector (shown in Fig. 3). It has been shown that h-BN detectors exhibit no response to gamma photons when directly exposed to a 662 keV Cesium-137 source.^{17,18,21} This is because BN is composed of low atomic number elements. However, the response of h-BN thick detectors to low energy (< 100 keV) gamma photons merits further investigation. Furthermore, it is known that nitrogen absorbs neutron via N-14(n,p)C-14 reaction, which has been utilized previously in GaN for detecting neutrons.³⁵ However, the N-14(n,p)C-14 reaction cross section of 2.4 Barn is negligibly small compared to a value of 3480 Barns of thermal neutron absorption cross section of ^{10}B in using h-BN for thermal neutron detection here.

The most important parameter for gauging the overall material quality is the charge collection efficiency itself. In a photodetector, the charge collection efficiency is defined as the ratio of the number of charge carriers collected by the electrodes to the total number of charge carriers generated. However, in the case of a semiconductor neutron detector, the neutron will be counted as long as the neutron-generated signal can trigger a voltage pulse above the low-level discriminator (LLD) setting in the electronics. Therefore, we use the deviation from the theoretically expected efficiency of Eq. (1) or the ratio of η/η_i as a measure of an effective charge collection efficiency for the purpose of gauging the material quality and device performance.

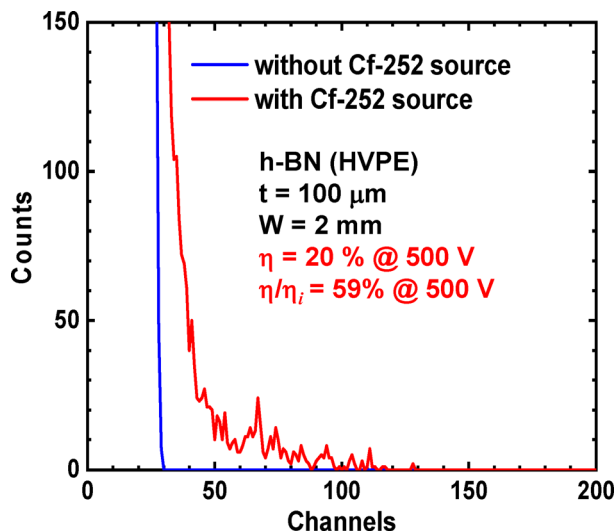


FIG. 4. Pulsed height spectra of the h-BN detector strip shown in Fig. 3 fabricated from a $100\ \mu\text{m}$ thick freestanding h-BN wafer grown by HVPE using natural boron trichloride (BCl_3) gas as a precursor, measured at 500 V. The red spectrum was measured under thermal neutron irradiation, and the blue spectrum was recorded in the absence of any radiation.

From the measured value of $\eta = 20\%$ and calculated value of η_i from Eq. (1) using the known thickness of $100\ \mu\text{m}$ and λ (h-BN) = $237\ \mu\text{m}$, we obtain a value of $\eta/\eta_i = 59\%$ at 500 V, while the prior state-of-the-art device ($100\ \mu\text{m}$ thick h- ^{10}BN thermal neutron detector with a detection efficiency of 59%) had a value of $\eta/\eta_i = 67\%$ at the same bias voltage of 500 V.²¹ Given the fact that the development of HVPE growth of h-BN semi-bulk wafers is at such an early stage, we believe that the demonstrated thermal neutron detector performance, including the measured detection efficiency of 20% and effective charge collection efficiency of 59%, represents a very significant milestone in the development of cost-effective h-BN semi-bulk crystals and h-BN semiconductor neutron detectors.

In summary, the established GaN semi-bulk crystal growth technique of HVPE has been utilized to produce natural h-BN semi-bulk wafers. Electrical transport characterization results revealed that these HVPE grown materials possess an electrical resistivity of $1 \times 10^{13}\ \Omega\ \text{cm}$, and a charge carrier mobility and lifetime product of $2 \times 10^{-4}\ \text{cm}^2/\text{V}\ \text{s}$. Detectors fabricated from these materials have shown to deliver a thermal neutron detection efficiency of 20%, corresponding to 59% of charge collection efficiency, at an operating voltage of 500 V. The results indicate that HVPE is a promising growth method to produce h-BN semi-bulk crystals and h-BN semiconductor neutron detectors at a reduced manufacturing cost. With further development, there is no question that h-BN detectors will replace the traditional He-3 gas detectors in certain application areas by offering obvious advantages of semiconductor technologies over gas detectors and opportunities for users to dedicate the scarce and expensive supply of He-3 gas to other application areas where substitutes of He-3 gas are not possible.

The research was supported by DOE ARPA-E (Nos. DE-AR0001257 and DE-AR0001552, monitored by Dr. Isik Kizilyalli, Dr. Olga Spahn, and Dr. Eric Carlson). Jiang and Lin are grateful to the AT&T Foundation for the support of Ed Whitacre and Linda Whitacre endowed chairs.

AUTHOR DECLARATIONS

Conflict of Interest

The authors have no conflicts to disclose.

Author Contributions

Z. Alemoush and N. K. Hossain contributed equally to this work.

Zaid Alemoush: Data curation (equal); Formal analysis (equal); Investigation (equal); Methodology (equal); Validation (equal); Visualization (equal). **Naymul K Hossain:** Data curation (equal); Formal analysis (equal); Investigation (equal); Methodology (equal); Validation (equal); Visualization (equal). **Attasit Tingsuwatit:** Data curation (equal); Formal analysis (equal); Investigation (equal); Methodology (equal); Validation (equal); Visualization (equal). **Musab Abdallah Almohammad:** Data curation (equal); Formal analysis (equal); Investigation (equal); Methodology (equal); Validation (equal); Visualization (equal). **Jing Li:** Data curation (equal); Formal analysis (equal); Investigation (equal); Methodology (equal); Software (equal); Supervision (equal); Validation (equal); Visualization (equal). **Jingyu Lin:** Conceptualization (equal); Data curation (equal); Formal analysis (equal); Funding acquisition (equal); Investigation (equal);

Methodology (equal); Project administration (equal); Resources (equal); Supervision (equal); Validation (equal); Visualization (equal); Writing – original draft (equal); Writing – review & editing (equal). **Hongxing Jiang:** Conceptualization (equal); Data curation (equal); Formal analysis (equal); Funding acquisition (equal); Investigation (equal); Methodology (equal); Project administration (equal); Resources (equal); Supervision (equal); Validation (equal); Visualization (equal); Writing – original draft (equal); Writing – review & editing (equal).

DATA AVAILABILITY

The data that support the findings of this study are available within the article.

REFERENCES

- ¹See <https://www.nobelprize.org/prizes/physics/2014/press-release/>. The Royal Swedish Academy of Sciences has decided to award the Nobel Prize in Physics for 2014 to Isamu Akasaki, Hiroshi Amano, and Shuji Nakamura.
- ²T. Sugino, K. Tanioka, S. Kawasaki, and J. Shirafuji, *Jpn. Appl. Phys., Part 2* **36**, L463 (1997).
- ³K. Watanabe, T. Taniguchi, and H. Kanda, *Nat. Mater.* **3**, 404 (2004).
- ⁴K. Watanabe, T. Taniguchi, and H. Kanda, *Nat. Photonics* **3**, 591 (2009).
- ⁵H. X. Jiang and J. Y. Lin, *Semicond. Sci. Technol.* **29**, 084003 (2014).
- ⁶N. Alem, R. Erni, C. Kisielowski, M. D. Rossell, W. Gannett, and A. Zettl, *Phys. Rev. B* **80**, 155425 (2009).
- ⁷L. Song, L. Ci, H. Lu, P. B. Sorokin, C. Jin, J. Ni, A. G. Kvashnin, D. G. Kvashnin, J. Lou, B. I. Yakobson, and P. M. Ajayan, *Nano Lett.* **10**, 3209 (2010).
- ⁸R. V. Gorbachev, I. Riaz, R. R. Nair, R. Jalil, L. Britnell, B. D. Belle, E. W. Hill, K. S. Novoselov, K. Watanabe, T. Taniguchi, A. K. Geim, and P. Blake, *Small* **7**, 465 (2011).
- ⁹L. Britnell, R. V. Gorbachev, R. Jalil, B. D. Belle, F. Schedin, A. Mishchenko, T. Georgiou, M. I. Katsnelson, L. Eaves, S. V. Morozov, N. M. R. Peres, J. Leist, A. K. Geim, K. S. Novoselov, and L. A. Ponomarenko, *Science* **335**, 947 (2012).
- ¹⁰T. T. Tran, C. Elbadawi, D. Totonjian, C. J. Lobo, G. Grosso, H. Moon, D. R. Englund, M. J. Ford, I. Aharonovich, and M. Toth, *ACS Nano* **10**, 7331 (2016).
- ¹¹N. R. Jungwirth, B. Calderon, Y. Ji, M. G. Spencer, M. E. Flatté, and G. D. Fuchs, *Nano Lett.* **16**, 6052 (2016).
- ¹²Z. Shotan, H. Jayakumar, C. R. Considine, M. Mackoite, H. Fedder, J. Wrachtrup, A. Alkauskas, M. W. Doherty, V. M. Menon, and C. A. Meriles, *ACS Photonics* **3**, 2490 (2016).
- ¹³M. Kianinia, B. Regan, S. A. Tawfik, T. T. Tran, M. J. Ford, I. Aharonovich, and M. Toth, *ACS Photonics* **4**, 768 (2017).
- ¹⁴O. Osberghaus, *Z. Phys.* **128**, 366 (1950).
- ¹⁵G. F. Knoll, *Radiation Detection and Measurement*, 4th ed. (John Wiley & Sons, 2010).
- ¹⁶S. J. Grenadier, A. Maity, J. Li, J. Y. Lin, and H. X. Jiang, “Electrical transport properties of hexagonal boron nitride epilayers,” in *Semiconductors and Semimetals*, edited by Y. Zhao (Elsevier, Amsterdam, 2021), Chap. 12.
- ¹⁷T. C. Doan, S. Majety, S. Grenadier, J. Li, J. Y. Lin, and H. X. Jiang, *Nucl. Inst. Methods Phys. Res., Sect. A* **748**, 84 (2014).
- ¹⁸A. Maity, T. C. Doan, J. Li, J. Y. Lin, and H. X. Jiang, *Appl. Phys. Lett.* **109**, 072101 (2016).
- ¹⁹A. Maity, S. J. Grenadier, J. Li, J. Y. Lin, and H. X. Jiang, *Appl. Phys. Lett.* **111**, 033507 (2017).
- ²⁰A. Maity, S. J. Grenadier, J. Li, J. Y. Lin, and H. X. Jiang, *Appl. Phys. Lett.* **114**, 222102 (2019).
- ²¹A. Maity, S. J. Grenadier, J. Li, J. Y. Lin, and H. X. Jiang, *Appl. Phys. Lett.* **116**, 142102 (2020).
- ²²I. C. Kizilyalli, O. B. Spahn, and E. P. Carlson, *ECS Trans.* **109**, 3 (2022).
- ²³D. S. McGregor, R. T. Klann, H. K. Gersch, and Y. H. Yang, *Nucl. Instrum. Methods Phys. Res., Sect. A* **466**, 126 (2001).
- ²⁴P. Lunca-Popa, J. I. Brand, S. Balaz, L. G. Rosa, N. M. Boag, M. Bai, B. W. Robertson, and P. A. Dowben, *J. Phys. D* **38**, 1248 (2005).
- ²⁵K. Osberg, N. Schemm, S. Balkir, J. O. Brand, M. S. Hallbeck, P. A. Dowben, and M. W. Hoffman, *IEEE Sensor J.* **6**, 1531 (2006).
- ²⁶R. J. Nikolic, A. M. Conway, C. E. Reinhardt, R. T. Graff, T. F. Wang, N. Deo, and C. L. Cheung, *Appl. Phys. Lett.* **93**, 133502 (2008).
- ²⁷A. M. Conway, T. F. Wang, N. Deo, C. L. Cheung, and R. J. Nikolic, *IEEE Trans. Nucl. Sci.* **56**, 2802 (2009).
- ²⁸R. Dahal, K. C. Huang, J. Clinton, N. LiCausi, J. Q. Lu, Y. Danon, and I. Bhat, *Appl. Phys. Lett.* **100**, 243507 (2012).
- ²⁹D. S. McGregor, S. L. Bellinger, R. G. Fronk, L. Henson, D. Huddleston, T. Ochs, J. K. Shultis, T. J. Sobering, and R. D. Taylor, *Radiat. Phys. Chem.* **116**, 32 (2015).
- ³⁰L. Weston, D. Wickramaratne, M. Mackoite, A. Alkauskas, and C. G. Van de Walle, *Phys. Rev. B* **97**, 214104 (2018).
- ³¹H. Fujikura, T. Konno, T. Kimura, Y. Narita, and F. Horikiri, *Appl. Phys. Lett.* **117**, 012103 (2020).
- ³²K. Ohnishi, N. Fujimoto, S. Nitta, H. Watanabe, S. Lu, M. Deki, Y. Honda, and H. Amano, *J. Appl. Phys.* **132**, 145703 (2022).
- ³³M. A. McKay, J. Li, J. Y. Lin, and H. X. Jiang, *J. Appl. Phys.* **127**, 053103 (2020).
- ³⁴A. Many, *J. Phys. Chem. Solids* **26**, 575 (1965).
- ³⁵J. Qiu, E. Katz, C. H. Lin, L. Cao, and L. J. Brillson, *Radiat. Eff. Defects Solids* **168**, 924 (2013).